Supplementary Information

A designed pyromellitic diimide derivative as negolyte for neutral aqueous organic redox flow battery with high power density

Weijie Zheng,[a] Yufeng Liu,[a] Mingbao Huang,[a,*] Kai Wan,[b] Zhipeng Xiang,[c] Zhiyong Fu,[a,d,*] and Zhenxing Liang[a]

[a] *Guangdong Provincial Key Laboratory of Fuel Cell Technology, School of Chemistry and Chemical Engineering, South China University of Technology, Guangzhou 510641, China.*

[b] *School of Chemical Engineering and Technology, Sun Yat-sen University, Zhuhai 519082, China.*

[c] *Institute for Sustainable Transformation, School of Chemical Engineering and Light Industry, Guangdong University of Technology, Guangzhou 510006, China.*

[d] *Beijing Laboratory of New Energy Storage Technology, Beijing 102206, China.*

*Corresponding authors, E-mail: huangmb08@hotmail.com, zyfu@scut.edu.cn

Experimental Section

1. Chemical

All of the reagents were purchased from commercial channels. Pyromellitic Dianhydride (96%, Shanghai Macklin Biochemical Technology Co., Ltd., China), pyromellitic diimide (97%, Shanghai Bide Pharmaceutical Technology Co., Ltd., China), monoethanolamine (99%, Shanghai Aladdin Bio-Chem Technology Co., Ltd., China), 3-bromo-*N*,*N*,*N*-trimethylpropan-1-aminium bromide (97%, Shanghai Bide Pharmaceutical Technology Co., Ltd., China), 1,4,5,8-naphthalenetetracarboxylic dianhydride (96%, Shanghai Macklin Biochemical Technology Co., Ltd., China), 3-(dimethylamino)-1-propylamine (99%, Shanghai Macklin Biochemical Technology Co., Ltd., China), *N*,*N*-dimethylaminomethylferrocene (98%, Anhui Senrise Technology Co., Ltd., China), 4,4′-bipyridine (98%, Shanghai Aladdin Bio-Chem Technology Co., Ltd., China), 1-chloro-2,4-dinitrobenzene (98%, Shanghai Adamas Reagent Co., Ltd., China), 4-amino-2,2,6,6-tetramethylpiperidine-1-oxyl (97%, Shanghai Aladdin BioChem Technology Co., Ltd., China), chloromethane (1 mol/L in THF, 99.5%, Anhui Senrise Technology Co., Ltd., China), iodomethane (99.5%, Anhui Senrise Technology Co., Ltd., China), *N*,*N*-dimethylformamide (99.9%, Shanghai Macklin Biochemical Technology Co., Ltd., China), dimethyl sulfoxide (99%, Shanghai Macklin Biochemical Technology Co., Ltd., China), ethanol (analytically pure, Sinopharm Chemical Reagent Co., Ltd., China), acetonitrile (analytically pure, Shanghai Lingfeng Chemical Reagent Co., Ltd., China), acetone (analytically pure, Guangzhou Chemical Reagent Factory, China), ether (analytically pure, Guangzhou Chemical Reagent Factory, China), tetrabutylammonium chloride (99%, Shanghai Adamas Reagent Co., Ltd., China), potassium hydroxide (99.99%, Shanghai Meryer Biochemical Technology Co., Ltd., China), potassium chloride (99.99%, Guangzhou Chemical Reagent Factory, China), potassium hexafluorophosphate (99%, Shanghai Aladdin Bio-Chem Technology Co., Ltd., China).

2. Synthesis

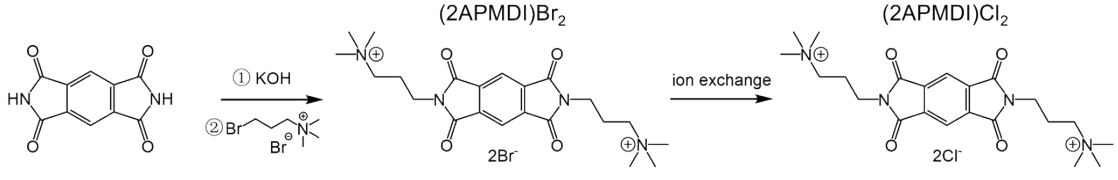

Scheme S1. Synthesis protocol of (2APMDI)Cl_2.

The (2APMDI)Cl_2 was synthesized via a straightforward one-step nucleophilic substitution reaction followed by an ion exchange (**Scheme S1**). In a 250 mL flask, a mixture of pyromellitic diimide (6.0 g, 27.8 mmol) and DMSO (100 mL) was stirred at 120℃ with balloon protection. When the solid was completely dissolved, a solution of KOH (3.9 g, 69.5 mmol) in ethanol (50 ml) was added into the mixture by dropwise over a period of 2 h. Then a solution of 3-bromo-*N*,*N*,*N*-trimethylpropan-1-aminium bromide (16.0 g, 61.3 mmol) in DMSO (30 ml) was added into the mixture and the reactant was stirred at 100℃ for 20 h. After cooling to room temperature, the mixture was filtered out and washed with DMSO and acetonitrile, and then dried under vacuum to afford 5,7-dihydro-N^2,N^2,N^2,N^6,N^6,N^6-hexamethyl-1,3,5,7-tetraoxobenzo[1,2-*c*:4,5-*c*′]dipyrrole-2,6(1*H*,3*H*)-dipropanaminium dibromide viz. (2APMDI)Br_2 (14.7 g, 91.9%, light yellow solid). Finally, (2APMDI)Br_2 was treated with ion exchange to obtain its chloride (2APMDI)Cl_2 (12.3 g, 94.8%, white solid).

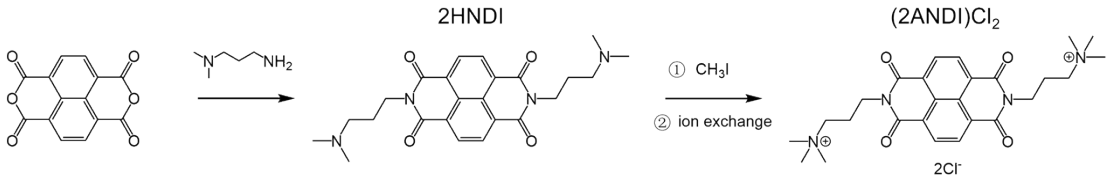

Scheme S2. Synthesis protocol of (2ANDI)Cl_2.

(2ANDI)Cl_2 was prepared using a modified procedure according to previous literature.[1]

In a 500 mL flask, a mixture of 1,4,5,8-naphthalene tetracarboxylic dianhydride (25.0 g, 93.2 mmol) and DMF (200 mL) was stirred at 150℃ with balloon protection. When the solid was completely dissolved, 3-(dimethylamino)-1-propylamine (35 ml, 278.1 mmol) was added into the mixture by dropwise over a period of 24 h. After cooling to room temperature, the mixture was filtered out and washed with DMF and acetone, and then dried under vacuum to afford 2,7-bis[3-(dimethylamino)propyl]benzo[*lmn*][3,8]phenanthroline-1,3,6,8(2*H*,7*H*)-tetrone viz. 2HNDI (33.5 g, 82.3%, golden solid).

In a 500 mL flask, a mixture of 2HNDI (15.0 g, 34.4 mmol) and CH_3I (24 mL, 385.5 mmol) in DMF (180 mL) was stirred at 80℃ for 48 h. After cooling to room temperature, the mixture was filtered out and washed with ethanol, and then dried under vacuum to afford benzo[*lmn*][3,8]phenanthroline-2,7-dipropanaminium,1,3,6,8-tetrahydro-N^2,N^2,N^2,N^7,N^7,N^7-hexamethyl-1,3,6,8-tetraoxo diiodide viz. (2ANDI)I_2 (19.7 g, 79.4%, red solid). Finally,

(2ANDI)I_2 was treated with ion exchange to obtain its chloride viz. (2ANDI)Cl_2 (9.9 g, 67.4%, white solid).

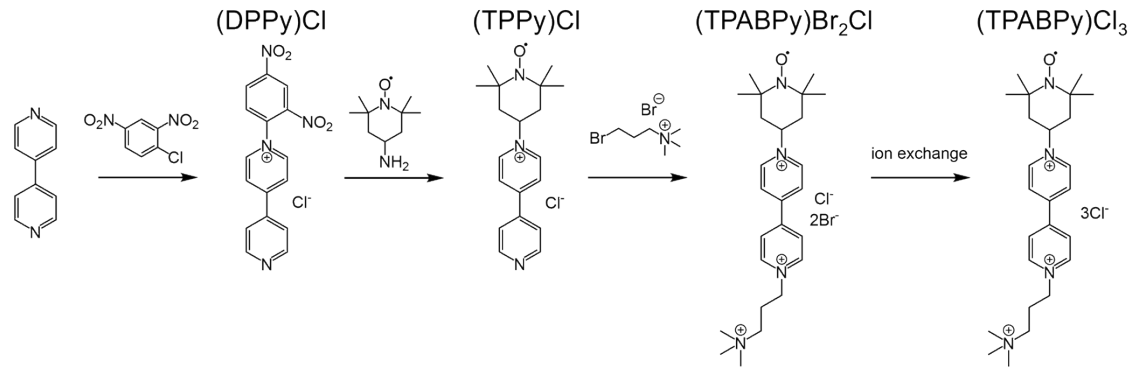

Scheme S3. Synthesis protocol of (TPABPy)Cl_3.

(TPABPy)Cl_3 was prepared using a modified procedure according to previous literature.[2]

In a 250 mL flask, a mixture consisting of acetone (250 mL), 1-choloro-2,4-dinitrobenzene (12.2 g, 60.0 mmol) and 4,4′-bipyridine (9.4 g, 60.0 mmol) was stirred at 75℃ for 12 h. After cooling to room temperature, the mixture was filtered out and washed with acetone, and then dried under vacuum to afford 1-(2,4-dinitrophenyl)-4-(4-pyridyl)pyridinium chloride) viz. (DPPy)Cl (19.9 g, 92.3%, grey solid).

In a 250 mL flask, (DPPy)Cl (14.3 g, 40.0 mmol) and 4-amino-2,2,6,6-tetramethylpiperidin-1-oxoyl (8.2 g, 48.0 mmol) were dissolved in ethanol-water solution (250 mL) with the volumetric ration of 4:1. The reactant was stirred at 90℃ for 12 h and then cooled to room temperature, and the orange-red filtrate was collected by vacuum filtration. The solvent was then removed by vacuum rotary evaporation. Acetone (150 mL) was added and refluxed at 70℃ for 6 h. The mixture was filtered out and washed with acetone to collect 1-(1-oxyl-2,2,6,6-tetramethylpiperidin-4-yl)-4-(4-pyri-dyl)pyridinium chloride viz. (TPPy)Cl (10.4 g, 74.7%, orange solid).

In a 250 mL flask, (TPPy)Cl (6.9 g, 20.0 mmol) and 3-bromo-*N*,*N*,*N*-trimethylpropan-1-aminium bromide (7.8 g, 30.0 mmol) were dispersed in DMF (60 mL) and stirred at 100℃ for 12 h. After cooling to room temperature, acetonitrile (200 mL) was added to the solution and the mixture was stirred for 3 h. The mixture was filtered out and washed with acetone to obtain 1-(1-oxyl-2,2,6,6-tetramethylpiperidin-4-yl)-1′-(3-(trimethylammonio)propyl)-4,4′-bipyridinium chloric dibromide viz. (TPABPy)Br_2Cl (10.1 g, 83.1%, orange solid). Finally, (TPABPy)Br_2Cl

was treated with ion exchange to obtain its chloride (TPABPy)Cl_3 (7.7 g, 89.2%, yellow solid).

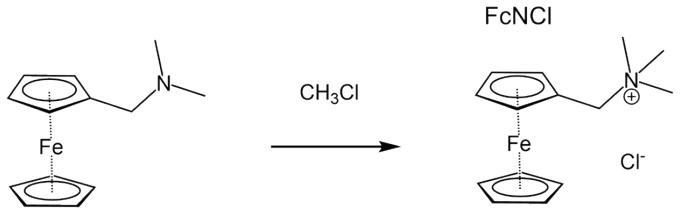

Scheme S4. Synthesis protocol of FcNCl.

FcNCl was prepared using a modified procedure according to previous literature.[3]

In a 250 mL flask, a mixture consisting of acetone (100 mL), *N*,*N*-dimethylaminomethylferrocene (25.0 g, 82.3 mmol) and chloromethane (100 ml, 100.0 mmol) was stirred at room temperature for 20 h. The mixture was filtered out and washed with ether, and then dried under vacuum to afford *N*,*N*,*N*-trimethylaminomethylferrocene chloride viz. FcNCl (23.1 g, 95.4%, yellow solid).

3. Nuclear magnetic resonance (NMR) spectra test

^{1}H NMR and ^{13}C NMR spectra were conducted on an AVANCE III HD 500 MHz (Bruker, Germany) by dissolving the compound in deuterium reagents.

4. Ultraviolet-visible (UV-vis) absorption spectra test

UV-vis spectra were collected on a Shimadzu UV-2600 spectrometer equipped with an optional integrating sphere.

5. Electron paramagnetic resonance (EPR) spectra test

EPR spectra were obtained using a Bruker ELEXSYS-II E500 CW-EPR (Bruker, Germany) spectrometer equipped with nitrogen.

6. Permeability measurement

A flow cell was used to evaluate the permeability across the DSV anion exchange membrane. The solution of 0.10 M (2APMDI)Cl_2 with 2.0 M KCl was filled in the donating side, and the 2.2 M KCl solution was filled in the receiving side. The electrolyte solutions were circulated through the cell by a peristaltic pump at a flow rate of 60 mL min^{-1}. Crossover of the

(2APMDI)Cl_2 was periodically monitored by taking 100 μL aliquot from the receiving side. The aliquot was diluted to the corresponding times and tested by UV-vis spectrometer. The concentration was quantified from the established calibration curve. The permeability was then calculated by the following equation:

$$P = \frac{C_t V_0 l}{At(C_0 - C_t)} \approx \frac{C_t V_0 l}{AtC_0}$$

where the P is the permeability ($cm^2\ s^{-1}$), V_0 is the initial volume of the receiving side (10 mL), A is the effective area of the membrane (9.0 cm^2), l is the thickness of the membrane (100 μm), t is time (s), C_t is the concentration measured at the receiving side at time t (M), C_0 is the initial concentration at the donating side (0.10 M).

7. Electrochemical test

Electrochemical tests were performed on a CHI 630E electrochemical workstation.

7.1 Cyclic voltammetry (CV) test

CVs were collected on a standard three-electrode system, including a glassy carbon disk (diameter of 3.0 mm) as the working electrode, an Ag/AgCl electrode as the reference electrode, and a platinum wire as the counter electrode.

7.2 Differential pulse voltammetry (DPV) test

DPVs were collected on a standard three-electrode system, including a glassy carbon disk (diameter of 3.0 mm) as the working electrode, an Ag/AgCl electrode as the reference electrode, and a platinum wire as the counter electrode. The experimental conditions were set as potential increase of 4 mV, amplitude of 50 mV, pulse width of 60 ms, sampling width of 20 ms and pulse period of 500 ms.

7.3 Linear sweep voltammetry (LSV) test

LSVs were collected on a standard three-electrode system, including a homemade Au ultramicroelectrode (diameter of 24.6 μm) as the working electrode, an Ag/AgCl electrode as the reference electrode, and a platinum wire as the counter electrode. The diffusion coefficient was calculated by using the steady-state current equation as follows:

$$i_{ss} = 4nFDC_0^* r_0$$

where i_{ss} is the steady-state current (A), n is the electron transfer number (1), F is the Faraday constant (96485 C mol^{-1}), D is the diffusion coefficient (cm^2 s^{-1}), C^*_0 is the bulk concentration of electroactive molecule (1.0 mM), r_0 is the radius of ultramicroelectrode (12.3 μm).

7.4 Digital Simulation

Details of the digital simulation are as follows:

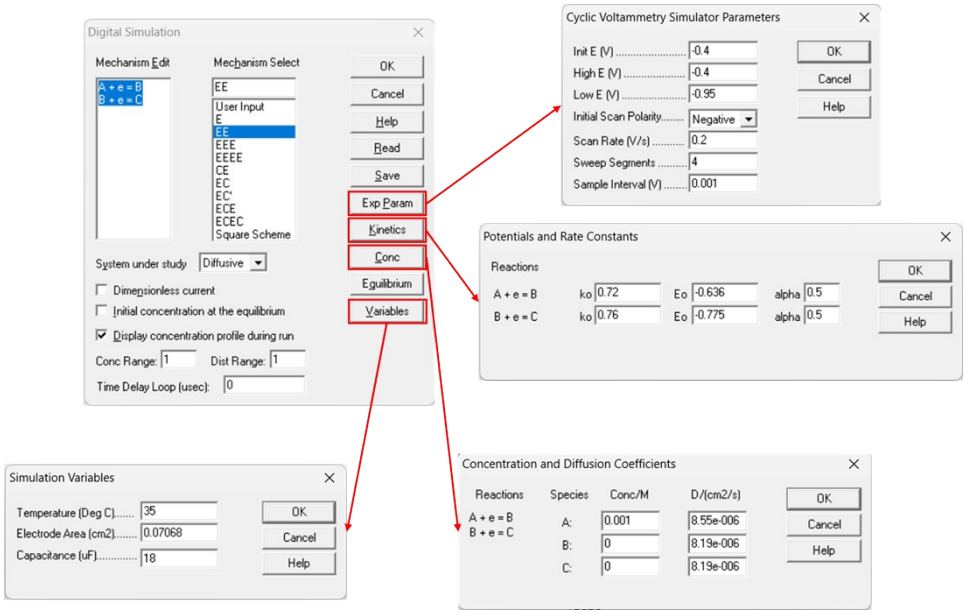

Scheme S5. The digital simulation programs of electron transfer rate constant (k_0) for (2APMDI)Cl_2.

8. Flow Battery Test

A laboratory-scale flow battery consisting of titanium collector plates, porous graphite felt electrodes (3 ⊠ 3 cm in size, 5 mm thickness), and commercial DSV anion-exchange membrane (AGC selemion) was assembled. The electrolytes were circulated through the cell by a peristaltic pump (Longer BT1002J) at a flow rate of 60 mL min^{-1}. The battery test was performed on a Neware BTS 3000 at room temperature in a glove box (Universal 2440/750/900) in an argon atmosphere (99.999%).

Test conditions for the rate and polarization: 7.0 mL negolyte of 0.35 M (2ANDI)Cl_2 or 0.35 M (2APMDI)Cl_2 with 1.5 M KCl and 12.0 mL posolyte of 0.30 M (TPABPy)Cl_3 with 1.4 M KCl were used. Cycling test for the 0.10 M flow battery: 7.0 mL negolyte of 0.10 M (2APMDI)Cl_2 with 2.5 M KCl and 14.0 mL posolyte of 0.10 M (TPABPy)Cl_3 with 2.3 M KCl

were used. Cycling test for the 1.0 M flow battery: 7.0 mL negolyte of 1.0 M (2APMDI)Cl_2 with 1.0 M KCl and 93.0 mL posolyte of 0.15 M (TPABPy)Cl_3 with 2.0 M KCl were used. The rate test of flow battery was conducted in a galvanostatic charge-discharge mode: (2ANDI)Cl_2 (0.30 – 1.35 V) and (2APMDI)Cl_2 (0.65 – 1.55 V). The cycling performance test was conducted in a galvanostatic charge-discharge mode with a cut-off voltage window of 0.30 – 1.70 V. The polarization curves were collected by galvanostatic discharging for 2 s at different current densities.

9. Density functional theory (DFT) calculation

All DFT calculations were performed by using the Gaussian 09 program.[4] The initial configurations were optimized at the B3LYP/6-311+G(d) level, including the empirical dispersion correction (GD3BJ),[5,6] with or without the implicit solvation model based on density (SMD). All optimized structures were checked by harmonic vibrational frequencies to ensure that they were on the minima of the potential energy surface (imaginary frequency = 0). The lowest unoccupied molecular orbital (LUMO), highest occupied molecular orbital (HOMO), spin density distribution and electrostatic potential of the optimized structure were analyzed by Multiwfn[7] and drawn by VMD[8] package.

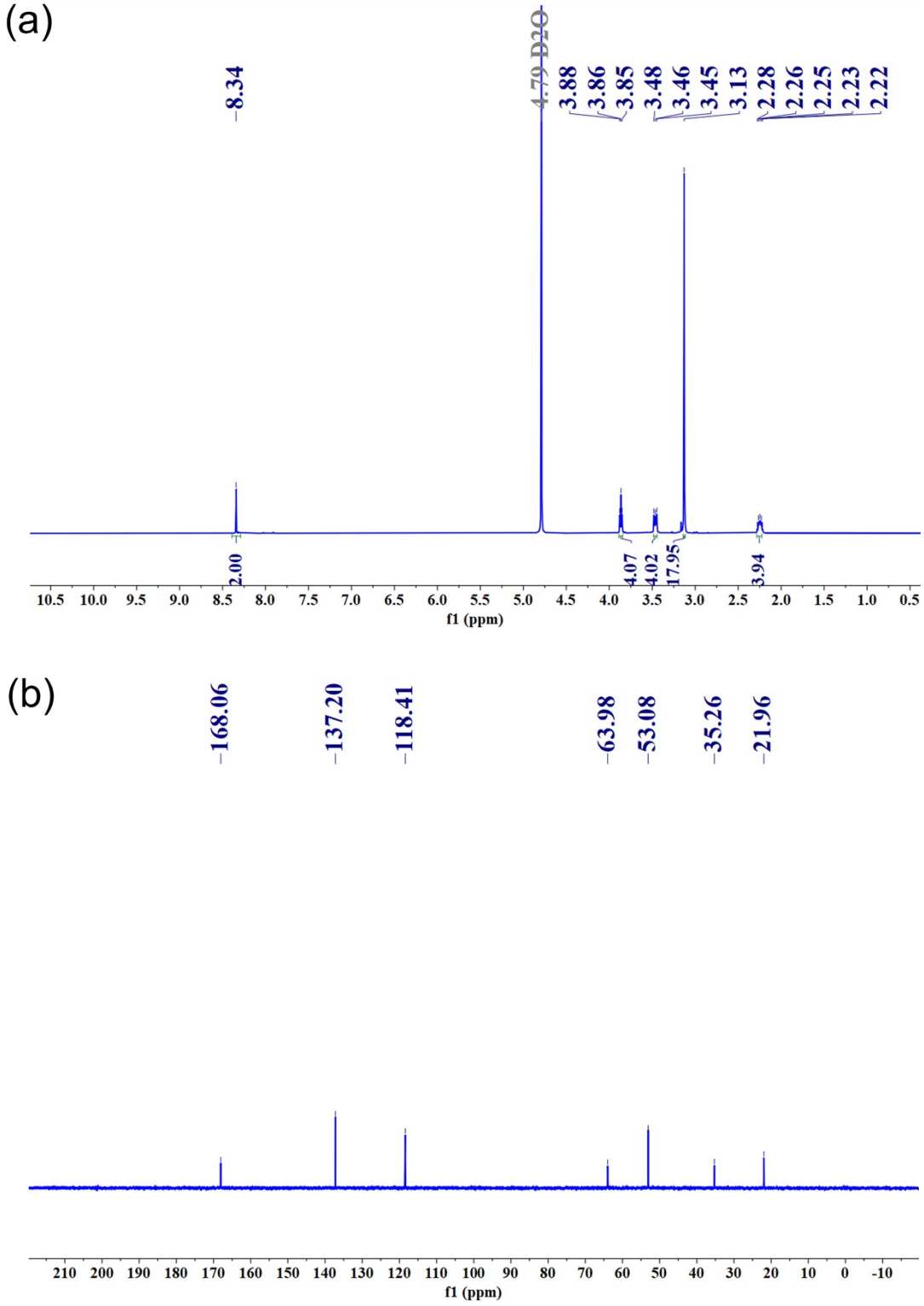

Figure S1. ^{1}H NMR spectrum (a) and ^{13}C NMR spectrum (b) of (2APMDI)Cl_2 (D_2O).

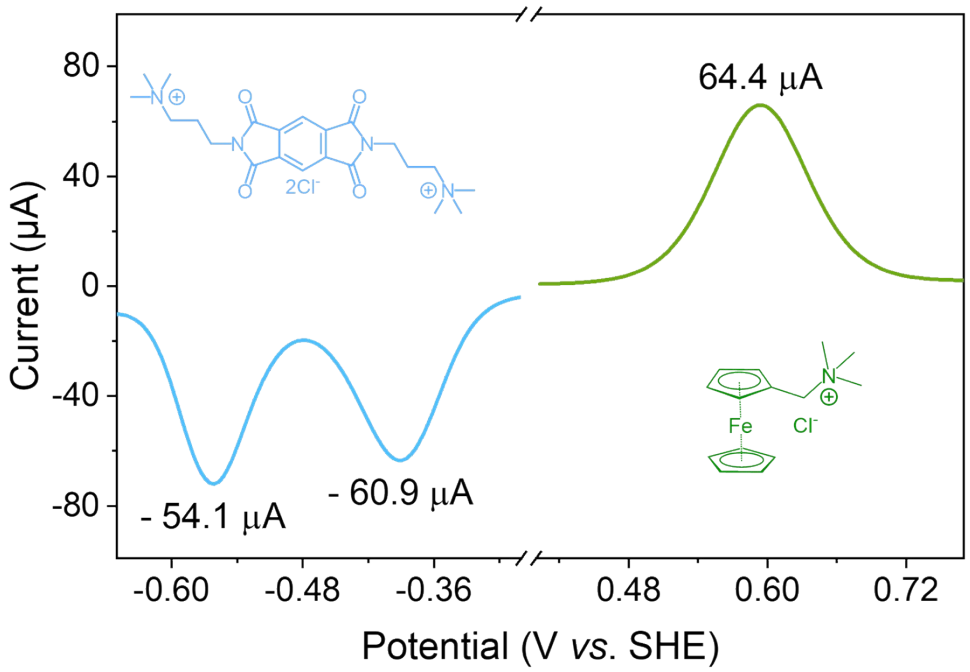

Figure S2. DPVs of 5.0 mM (2APMDI)Cl_2 and 5.0 mM FcNCl in 1.0 M KCl solution.

The electron-transferred number (n) of (2APMDI)Cl_2 is confirmed by DPVs. Here, the FcNCl is used as a standard compound whose n is considered as 1.[9–12] As shown in **Figure S2**, the (2APMDI)Cl_2 shows two consecutive reduction processes with similar peak currents. The reduction peak currents of (2APMDI)Cl_2 are close to the oxidation peak current of FcNCl, indicating that the (2APMDI)Cl_2 undergoes two consecutive single-electron reduction processes.

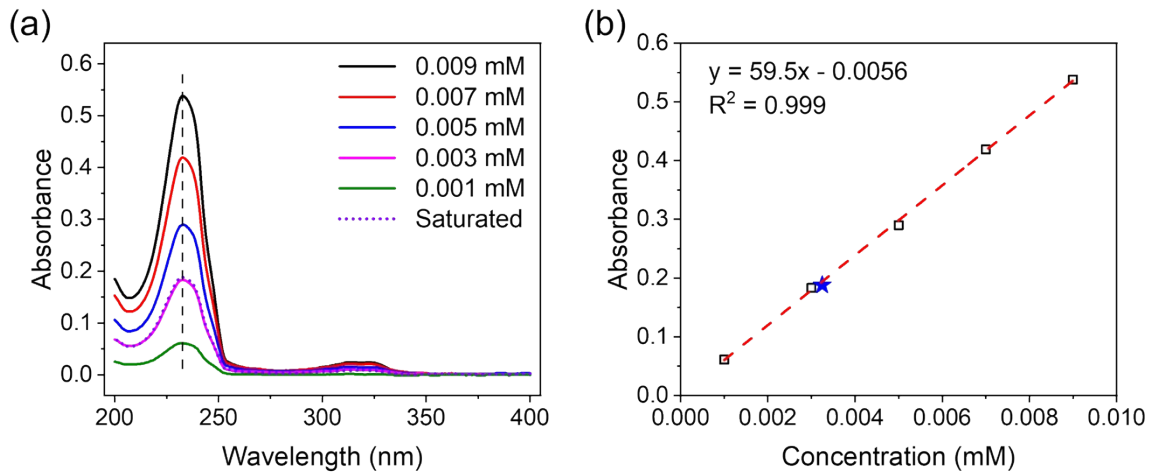

Figure S3. (a) UV-vis spectra of (2APMDI)Cl_2 at different concentrations. (b) UV-vis standard curve of (2APMDI)Cl_2.

The standard curve was established by plotting the concentration *versus* absorbance, and the absorbance at 233 nm was used to quantify the concentration based on the Lambert-Beer law.

The saturated solution of (2APMDI)Cl_2 in water was diluted 1000000 times and the absorbance was collected (blue star). The S was calculated as follows:

$$S = \frac{(0.188 + 0.0056)}{59.5} \times 1000000\ mM = 3.25\ M$$

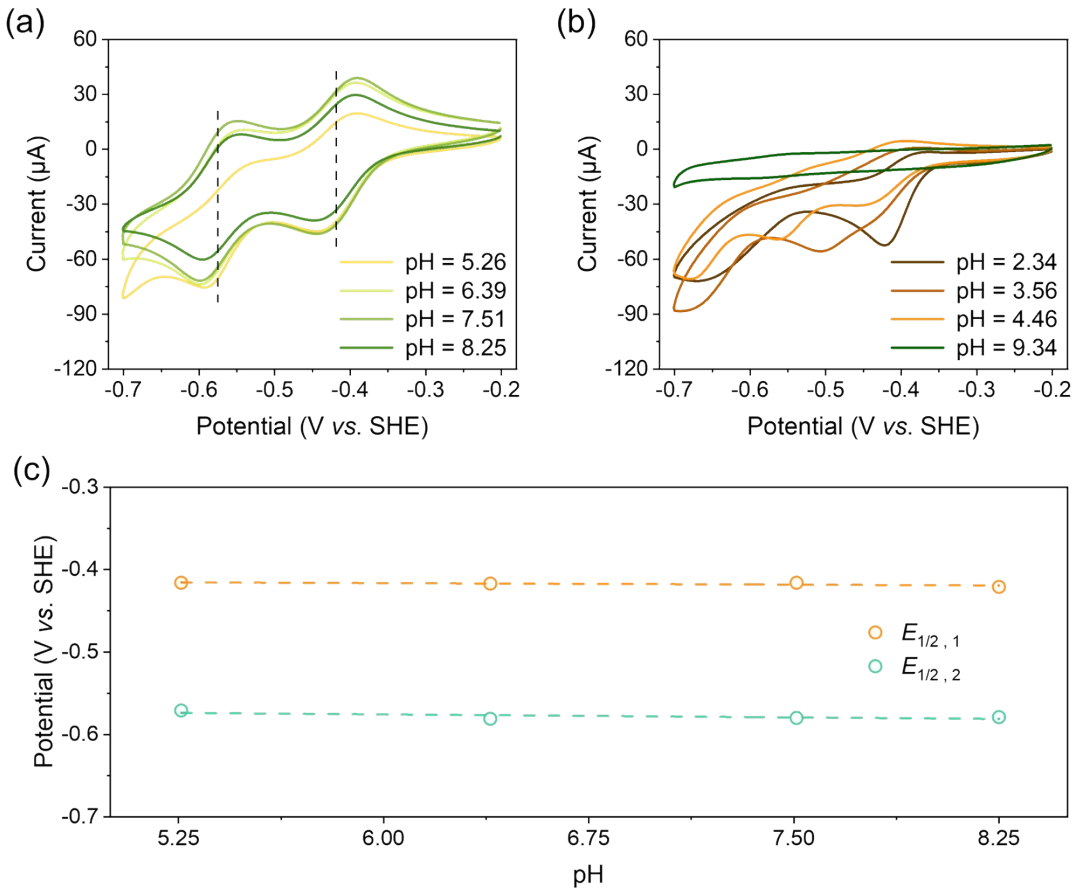

Figure S4. (a) and (b) CVs of 2.0 mM (2APMDI)Cl_2 in 0.50 M KCl solution at different pH (0.10 M buffer solution, scan rate: 200 mV s^{-1}). (c) The corresponding Pourbaix diagram of (2APMDI)Cl_2.

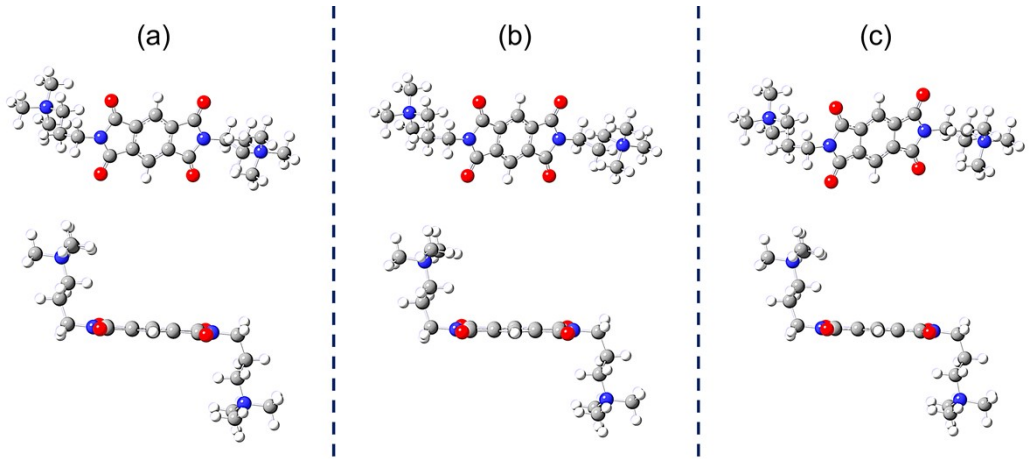

Figure S5. The geometric structures of (a) $2APMDI^{2+}$, (b) $2APMDI^{\bullet+}$ and (c) 2APMDI by DFT calculations.

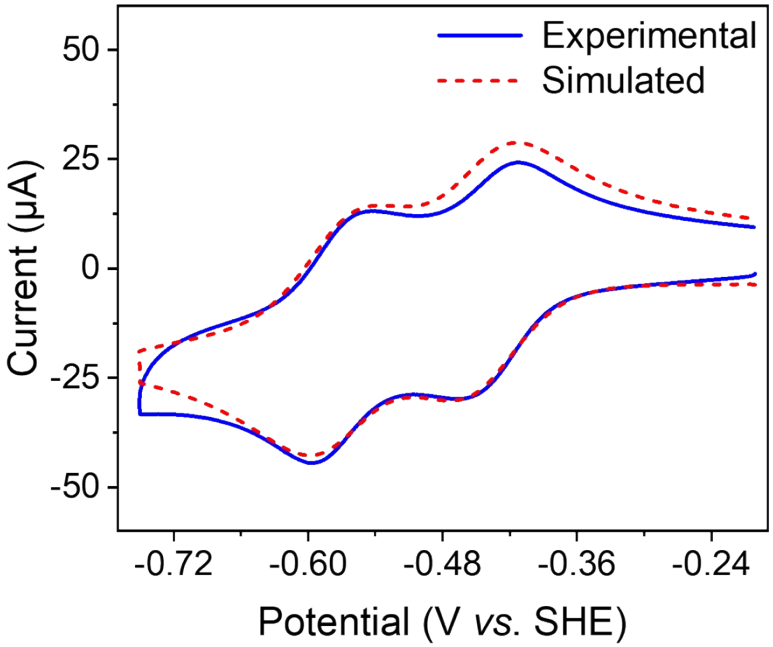

Figure S6. CV of 1.0 mM (2APMDI)Cl_2 in 1.0 M KCl solution (scan rate: 200 mV s^{-1}) and the corresponding simulation result.

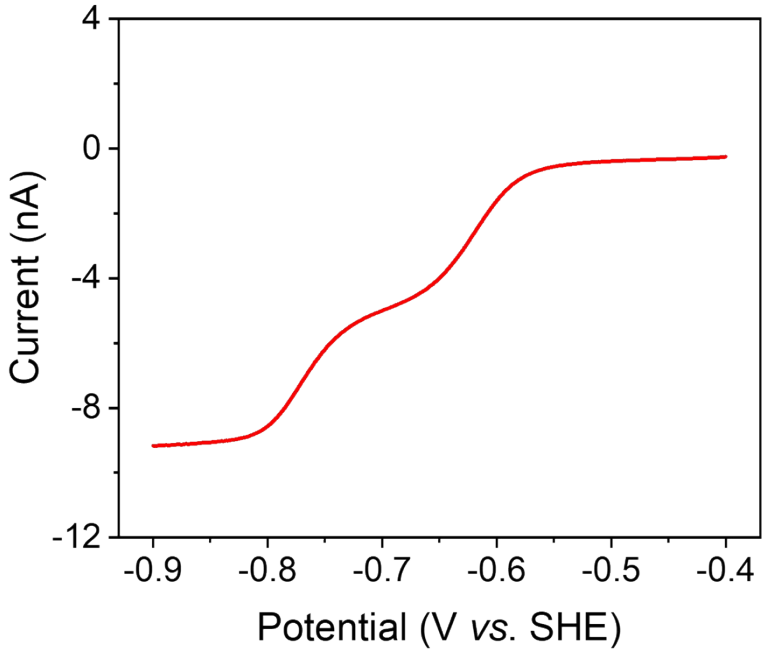

Figure S7. LSV of 1.0 mM (2APMDI)Cl_2 in 1.0 M KCl solution (scan rate: 50 mV s^{-1}).

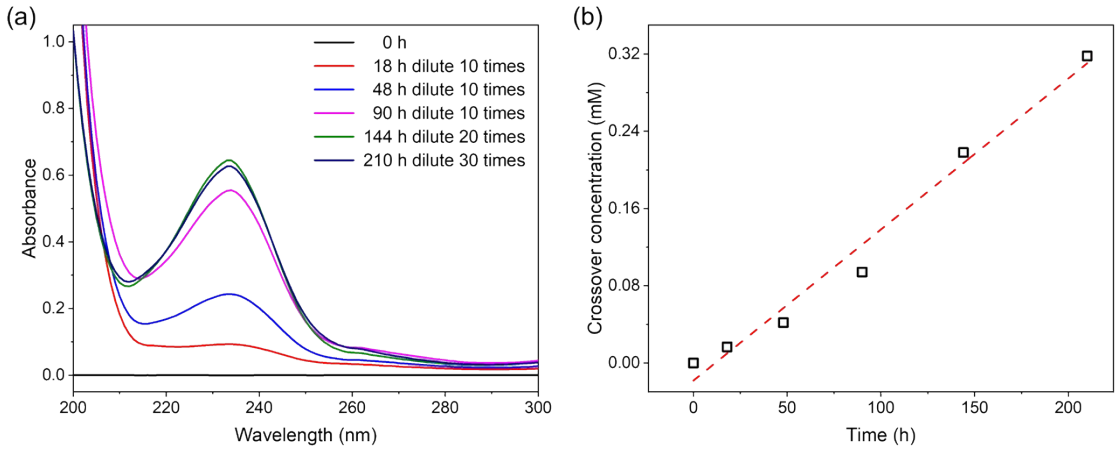

Figure S8. (a) UV-vis spectra of the solution in the receiving side. (b) Crossover concentration *versus* time.

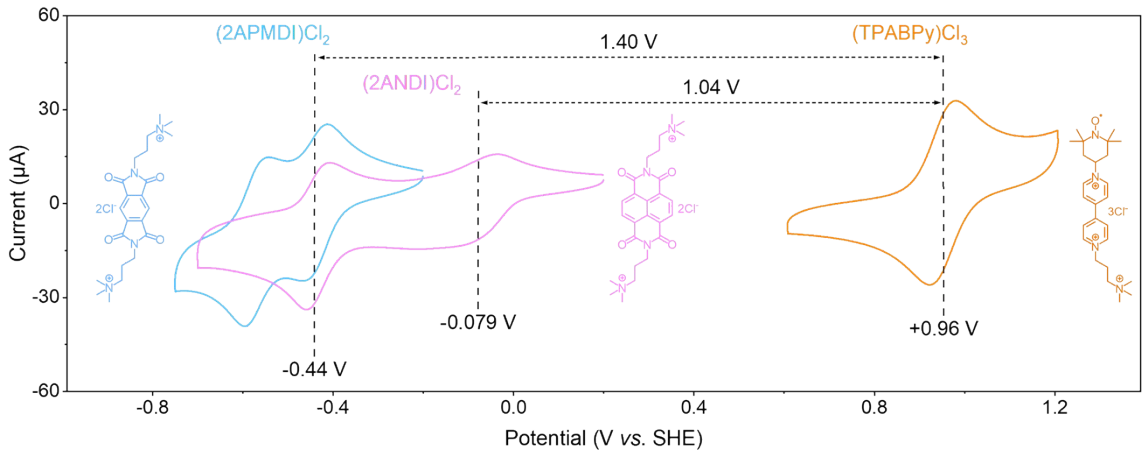

Figure S9. CVs of 1.0 mM $(2APMDI)Cl_2$, $(2ANDI)Cl_2$, and $(TPABPy)Cl_3$ in 1.0 M KCl solution at a scan rate of 200 mV s^{-1}.

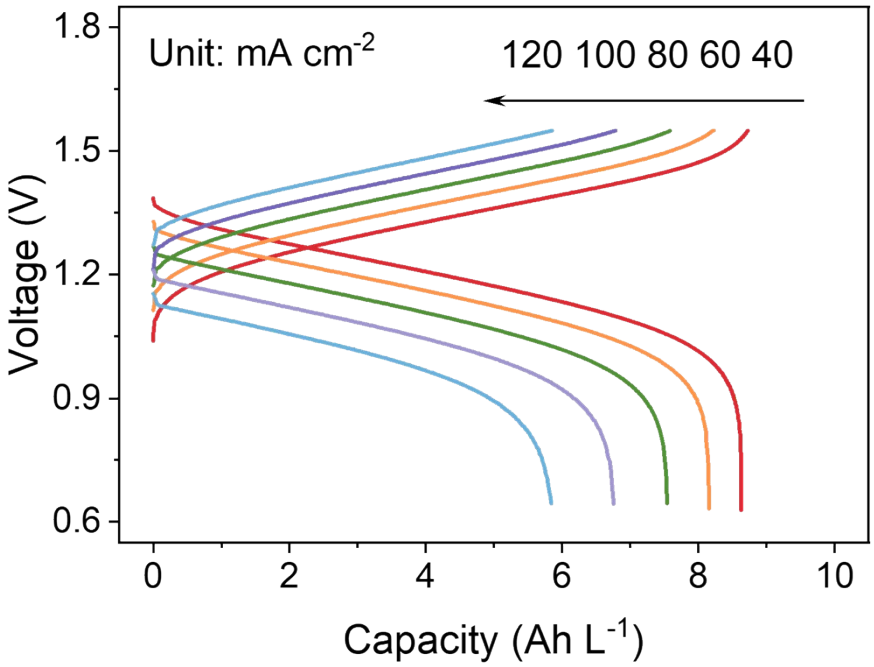

Figure S10. Galvanostatic charge and discharge profiles of 0.35 M (2APMDI)Cl_2-based flow battery operated at different current densities.

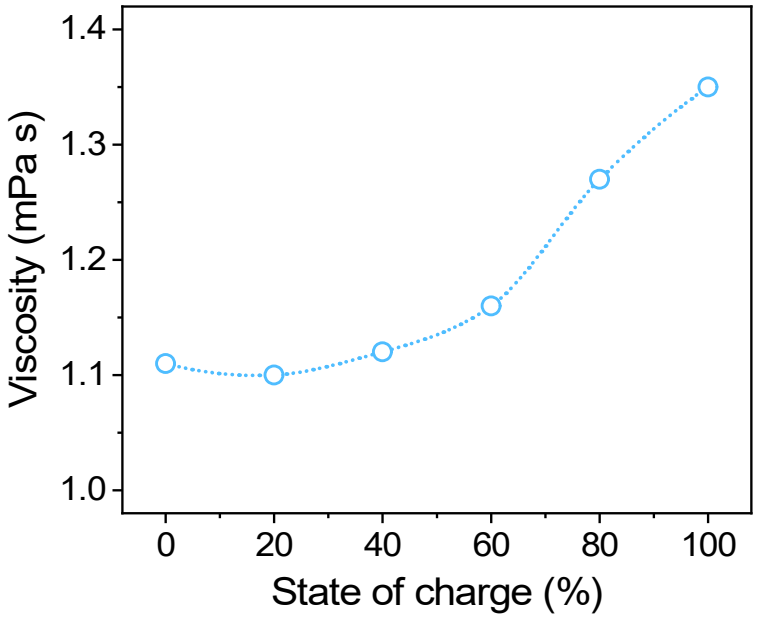

Figure S11. Viscosity of 0.35 M (2APMDI)Cl_2 electrolyte at different SOCs.

Table S1. A summary of physicochemical parameters of $(2APMDI)Cl_2$ and $(2ANDI)Cl_2$.

Compound	$E_{1/2}$ (V *vs*. SHE)	k_0 (cm s^{-1})	D (10^{-6} cm^2 s^{-1})
$(2APMDI)Cl_2$	-0.44; -0.58	0.72; 0.76	8.55; 8.19
$(2ANDI)Cl_2$	-0.08; -0.43	0.042; 0.015 [1]	4.02; 1.84[1]

Table S2. A summary of aromatic diimides for aqueous organic redox flow battery.

Compound	Solubility (M)	$E_{1/2}$ (V *vs*. SHE)	Energy efficiency (%)	Power density (mW cm^{-2})	Operating concentration (M)	Capacity degradation (% per cycle)	Testing temperature (°C)	Reference
K_2-BNDI	0.167	-0.18, -0.43	58 (20 mA cm^{-2})	37	0.025	0.168	25	[13]
2H-NDI	NA	-0.066, -0.41	22 (60 mA cm^{-2})	NA	0.50	0.275	NA	[14]
2DMA-NDI	NA	-0.31	55 (60 mA cm^{-2})	NA	0.050	0.00509	NA	[14]
GABA-NDI	0.587	-0.12, -0.43	81 (60 mA cm^{-2})	NA	0.20	0.0145	NA	[15]
PDI	0.08 (2 M NaCl)	-0.13, -0.45	NA	NA	0.020	0.00127	NA	[16]
TPDI	0.14 (2 M NaCl)	-0.17, -0.35	41 (70 mA cm^{-2})	83	0.10	0.0139	NA	[16]
A^{2+}-*Et*-NDI	0.7	-0.24, -0.54	69 (10 mA cm^{-2})	28	0.30	0.0667	NA	[17]
$4A^{4+}$-NDI	1.5	-0.21, -0.50	29 (50 mA cm^{-2})	22	1.0	0.00400	NA	[18]
[ANDI]Cl_2	1.0	-0.012, -0.44	50 (80 mA cm^{-2})	179	0.25	0.00230	NA	[1]
[HANDI]Cl_2	0.78	-0.014, -0.44	71 (40 mA cm^{-2})	NA	0.25	0.00394	NA	[1]
NDI-DMe	0.92	-0.41	48 (100 mA cm^{-2})	128	0.50	0.398	NA	[19]

"NA" represents data unavailable.

Table S2.(continued) A summary of aromatic diimides for aqueous organic redox flow battery.

Compound	Solubility (M)	$E_{1/2}$ (V *vs*. SHE)	Energy efficiency (%)	Power density (mW cm^{-2})	Operating concentration (M)	Capacity degradation (% per cycle)	Testing temperature (°C)	Reference
NDI-DEtOH	0.94	-0.37	50 (100 mA cm^{-2})	132	0.50	0.271	NA	[19]
siol-NDI	1.60	-0.08, -0.44	38 (100 mA cm^{-2})	157	1.0	0.0244	NA	[20]
diol-NDI	2.13	-0.09, -0.45	40 (100 mA cm^{-2})	150	1.0	0.0388	NA	[20]
dex-NDI	1.85	-0.09, -0.42	50 (100 mA cm^{-2})	203	1.0	0.00520	NA	[20]
$(SPrOH)_2NDI$	0.31	-0.11, -0.44	NA	NA	NA	NA	NA	[21]
$(SPr)_2NDI$	0.69	-0.11, -0.43	41 (100 mA cm^{-2})	119	0.25	0	25	[21]
$(CBu)_2NDI$	1.49	-0.11, -0.44	47 (100 mA cm^{-2})	165	1.0	0	25	[21]
NDI-C_2-MzMe	0.59	-0.07, -0.41	42 (100 mA cm^{-2})	129	0.40	0.0374	NA	[22]
NDI-C_3-MzMe	1.26	-0.09, -0.44	62 (100 mA cm^{-2})	206	1.0	0.0441	NA	[22]
NDI-C_3-MzOH	1.43	-0.08, -0.44	55 (100 mA cm^{-2})	235	1.0	0.0195	NA	[22]
$(2APMDI)Cl_2$	3.25	-0.44, -0.58	74 (100 mA cm^{-2}) 69 (120 mA cm^{-2})	307	1.0	0.0145	25	This work

"NA" represents data unavailable.

References

1 M. Pan, W. Wang, H. Wang, J. Ma, M. Shao and Z. Jin, *J. Power Sources*, 2023, **580**, 233269.

2 S. Hu, L. Wang, X. Yuan, Z. Xiang, M. Huang, P. Luo, Y. Liu, Z. Fu and Z. Liang, *Energy Mater. Adv.*, 2021, **2021**, 9795237.

3 J. Luo, M. Hu, W. Wu, B. Yuan and T. L. Liu, *Energy Environ. Sci.*, 2022, **15**, 1315–1324.

4 Frisch, M. J.; Trucks, G. W.; Schlegel, H. B.; Scuseria, G. E.; Robb, M. A.; Cheeseman, J. R.; Scalmani, G.; Barone, V.; Petersson, G. A.; Nakatsuji, H.; Li, X.; Caricato, M.; Marenich, A.; Bloino, J.; Janesko, B. G.; Gomperts, R.; Mennucci, B.; Hratchian, H. P.; Ortiz, J. V.; Izmaylov, A. F.; Sonnenberg, J. L.; Williams-Young, D.; Ding, F.; Lipparini, F.; Egidi, F.; Goings, J.; Peng, B.; Petrone, A.; Henderson, T.; Ranasinghe, D.; Zakrzewski, V. G.; Gao, J.; Rega, N.; Zheng, G.; Liang, W.; Hada, M.; Ehara, M.; Toyota, K.; Fukuda, R.; Hasegawa, J.; Ishida, M.; Nakajima, T.; Honda, Y.; Kitao, O.; Nakai, H.; Vreven, T.; Throssell, K.; Montgomery, J. A.; Jr., Peralta, J. E.; Ogliaro, F.; Bearpark, M.; Heyd, J. J.; Brothers, E.; Kudin, K. N.; Staroverov, V. N.; Keith, T.; Kobayashi, R.; Normand, J.; Raghavachari, K.; Rendell, A.; Burant, J. C.; Iyengar, S. S.; Tomasi, J.; Cossi, M.; Millam, J. M.; Klene, M.; Adamo, C.; Cammi, R.; Ochterski, J. W.; Martin, R. L.; Morokuma, K.; Farkas, O.; Foresman, J. B. Fox,; D. J. Gaussian 09, Revision A.02, *Gaussian*, *Inc.*, *Wallingford CT*, 2009.

5 S. Grimme, *J. Comput. Chem.*, 2004, **25**, 1463–1473.

6 S. Grimme, S. Ehrlich and L. Goerigk, *J. Comput. Chem.*, 2011, **32**, 1456–1465.

7 T. Lu and F. Chen, *J. Comput. Chem.*, 2012, **33**, 580–592.

8 W. Humphrey, A. Dalke and K. Schulten, *J. Mol. Graph.*, 1996, **14**, 33–38.

9 J. Gao, K. Amini, T. Y. George, Y. Jing, T. Tsukamoto, D. Xi, R. G. Gordon and M. J. Aziz, *Adv. Energy Mater.*, 2022, **12**, 2202444.

10 Q. Chen, Y. Li, Y. Liu, P. Sun, Z. Yang and T. Xu, *ChemSusChem*, 2021, **14**, 1295–1301.

11 B. Hu, C. DeBruler, Z. Rhodes and T. L. Liu, *J. Am. Chem. Soc.*, 2017, **139**, 1207–1214.

12 X. Li, P. Gao, Y.-Y. Lai, J. D. Bazak, A. Hollas, H.-Y. Lin, V. Murugesan, S. Zhang, C.-F. Cheng, W.-Y. Tung, Y.-T. Lai, R. Feng, J. Wang, C.-L. Wang, W. Wang and Y. Zhu, *Nat. Energy*, 2021, **6**, 873–881.

13 V. Medabalmi, M. Sundararajan, V. Singh, M.-H. Baik and H. R. Byon, *J. Mater. Chem. A*, 2020, **8**, 11218–11223.

14 C. Wiberg, L. Evenäs, M. Busch and E. Ahlberg, *J. Electroanal. Chem.*, 2021, **896**, 115224.

15 M. Shahsavan, C. Wiberg and P. Peljo, *Chem. Commun.*, 2022, **58**, 12692–12695.

16 X. Liu, X. Zhang, C. Bao, Z. Wang, H. Zhang, G. Li, N. Yan, M.-J. Li and G. He, *CCS Chem.*, 2023, **5**, 2334–2347.

17 V. Singh, S. Ahn and H. R. Byon, *Batteries Supercaps*, 2022, **5**, e202200281.

18 V. Singh, S. Kwon, Y. Choi, S. Ahn, G. Kang, Y. Yi, M. H. Lim, J. Seo, M. Baik and H. R. Byon, *Adv. Mater.*, 2023, **35**, 2210859.

19 Z. Wang, X. Liu, X. Zhang, H. Zhang, Y. Zhao, Y. Li, H. Yu and G. He, *Mater. Horiz.*, 2024, **11**, 1283–1293.

20 X. Liu, H. Zhang, C. Liu, Z. Wang, X. Zhang, H. Yu, Y. Zhao, M. Li, Y. Li, Y. He and G. He, *Angew. Chem. Int. Ed.*, 2024, **63**, e202405427.

21 H. Zhang, C. Liu, Z. Wang, X. Liu, Z. Han, X. Zhang, Y. Li, Q. Zhao and G. He, *Natl. Sci. Rev.*, 2025, **12**, nwaf123.

22 X. Zhang, X. Liu, Z. Wang, C. Liu, H. Zhang, H. Yu, Q. Zhao and G. He, *Energy Storage Mater.*, 2025, **81**, 104527.